Two-Charged-Particle Final States of K^-p Interactions at 2.63 and 2.70 GeV/c*

J. R. FICENEC,† H. A. GORDON, AND W. P. TROWER†
Department of Physics, University of Illinois, Urbana, Illinois
(Received 4 June 1968)

We have studied 16 138 two-prong events at an averaged-incident kaon momentum of 2.66 GeV/c, using the 72-in. hydrogen bubble chamber and scanning and measuring projectors to determine the total and partial cross sections for the contributing reactions. For elastic scattering, we measured the production distribution and fitted it with several models. We studied the production and decay distributions for the $\bar{K}^*N$ final states and obtained the effective-mass distributions for the three-body final states.

I. INTRODUCTION

STRUCTURE in the various final states produced by negative kaons of momentum between 1 and 2 GeV/c, observed in the 72-in. liquid-hydrogen bubble chamber, led the Alvarez group to extend their investigation up to 2.7 GeV/c. A separated beam for this purpose was designed and built in 1964, and the exposure which is analyzed here was obtained subsequently.[1] As part of a general Berkeley-Illinois collaboration, we have scanned more than 65 rolls of film at 2.63 and 2.70 GeV/c for all events and have measured the two-prong, two-prong with a kink on the positive or negative secondary, four-prong, and four-prong with a kink on the positive or negative secondary topologies. The data reported here involve the analysis of the two-prong topology at two different beam momenta, 2.63 and 2.70 GeV/c, which have been combined for analysis. We report the total, elastic, and some three-body and quasi-two-body final-state cross sections. We compare the cross sections and angular distributions for the elastic and quasi-two-body final states with other experiments. The final results for the elastic-scattering final state are not significantly different from those reported elsewhere.[2]

II. EXPERIMENTAL PROCEDURE

A. Scanning and Measuring

The data which have been analyzed are present on 65 rolls of 46-mm film, each roll containing about 600 sets of stereoscopic triads. The total exposure had approximately 39 000 of such triads, each displaying on the average eight-beam tracks.

The scanning and measuring procedures used here were similar to those in our experiment[3] at 1.33 GeV/c. The scanning efficiencies which were calculated on the assumption that events were missed at random ranged between 90 and 99% for various topologies.

The two-prong measurements were fitted to the mass hypotheses listed in Table III with the result that 60% (16 138 events) were fit with a 1% confidence level or better after two attempts at measurement. This low percentage was a result of our refusal to measure events in the first 15 and last 10 cm of the 165 cm of path length (15%), the measuring failures for valid kaon-produced events (10%), the loss in scanning for small-angle elastic scatters (8%), computer malfunctions when preparing measurement lists (4%), the failure of pion-produced events (2%), and the loss due to scanning inefficiency (1%).

B. Beam Characteristics

The beam momentum at each of the two magnet settings was determined by analyzing a sample of three-prong events which fit the mass hypothesis of the τ-decay mode of the K^- meson. The momenta corresponding to these two determinations were $P_{\text{beam}} = 2.63 \pm 0.03$ and $= 2.70 \pm 0.03$ GeV/c. The data at these two momenta were combined for the purpose of this analysis because their momenta overlapped and the results using the combined sample were consistent with those of each separately.

The beam composition was determined by counting the number of δ rays whose radius exceeded that which could be produced by kaons of the beam energy and by counting the subsequent strong interactions associated with these beam tracks. No electrons were expected in the beam since they would suffer on the average a 0.9-GeV energy loss while traversing the 0.25-in. stainless-steel window.[4] As a check of these results the number of kaon-produced τ decays was counted. These numbers were in agreement within the statistical errors for the fraction of beam kaons. Table I summarizes the results of the study of the beam characteristics.

C. Detection and Measurement Biases

Biases in the detection and measurement of events which were encountered are summarized now and

* Work supported by the U. S. Atomic Energy Commission. Funds for operation of the computer provided in part by the National Science Foundation.
† Present address: Physics Department, Virginia Polytechnic Institute, Blacksburg, Va. 24061.
[1] D. W. Merrill and J. Button-Shafer, Phys. Rev. **167**, 1202 (1968).
[2] J. R. Ficenec and W. P. Trower, Phys. Letters, **25B**, 369 (1967).
[3] W. P. Trower, J. R. Ficenec, R. I. Hulsizer, J. Lathrop, J. N. Snyder, and W. P. Swanson, Phys. Rev. **170**, 1207 (1968).
[4] W. P. Trower, Lawrence Radiation Laboratory Report No. UCRL-2426, Vol. IV, 1965 (unpublished).

TABLE I. Beam characteristics.

Beam momentum (GeV/c)	2.63±0.03	2.70±0.03
% kaons	88.7 ±2.4	81.2 ±4.1
% pions	8.1 ±1.4	11.8 ±2.9
% muons	3.2 ±1.9	7.0 ±2.8
τ decays expected	715 ±18	226 ±10
τ decays seen	755 ±28	224 ±15

discussed in detail elsewhere.[2,3] The smallest value of the scattering angle in the film plane that could be reliably detected by the scanners corresponds to $\cos\theta_p = 0.975$, where

$$\cos\theta_p = \hat{P}_{K^-\text{in}} \cdot \hat{P}_{K^-\text{out}} \tag{1}$$

in the over-all c.m. system. We estimated the number of elastic scattering events missed by correcting the angular distribution for azimuthal biases in the interval $0.875 \leq \cos\theta_p \leq 0.975$. We then fit the angular distribution as seen in Fig. 1 in the region $0.7 \leq \cos\theta_p \leq 0.975$ by the function

$$N(\theta) = \exp[C(\cos\theta_p - 1)]. \tag{2}$$

We assume further that the true distribution is represented in the depleted region by the extrapolation of this function $N(\theta)$.

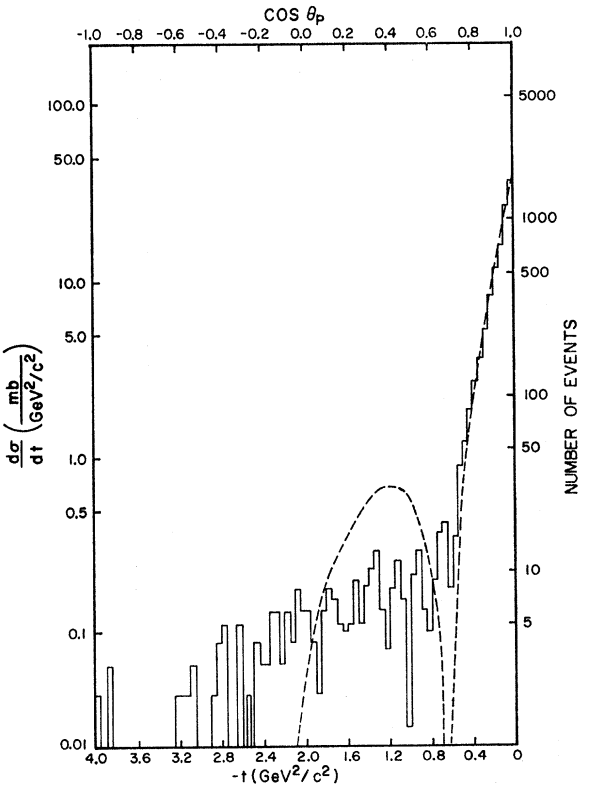

FIG. 1. Kaon elastic differential-scattering cross section. The dashed curve is the fit to the function given in Eq. (5), where $\alpha = 0.25 \pm 0.03$ and $R = 0.94 \pm 0.04$ F.

TABLE II. Summary of cross-section data.

Quantity	Beam momentum (GeV/c) 2.63±0.03	2.70±0.03	2.66±0.07
Stereoscopic triads	27 000	12 000	39 000
Path length (km)	355	161	516
No. of beam tracks	215 000	98 000	313 000
No. of interactions	32 400	14 500	46 900
σ_{tot} (mb)	30.3±1.2	30.9±2.2	30.4±1.0

The probability of occurrence of prompt, slow, and neutral decays which will change the characteristic scan topology to which an event is assigned can be computed from known lifetimes and branching ratios of the measured final-state particles and the chamber geometry. By using the number of events with unstable particles that are found in their characteristic topology, we estimate the number of events that appear in unusual topologies and when measured pass an erroneous-mass hypothesis. This type of contaminant which constituted a considerable percentage of some final states [e.g., $\bar{K}^0 p\pi^-$ (20%), $\Lambda^0\pi^+\pi^-$ (14%), $\Sigma^0\pi^+\pi^-$ (13%), and $\pi^+\pi^-$MM (40%)] was corrected for when calculating the partial cross sections.

III. EXPERIMENTAL RESULTS

A. Total K^-p Cross Section

The total cross section was computed by dividing the number of interactions found, corrected for scan inefficiencies, by the total path length of beam particles within the fiducial volume of the chamber and using the density and weight of liquid hydrogen. This procedure is discussed in more detail elsewhere[3] and results are summarized in Table II.

B. Classification of Events

To determine the partial cross sections and angular distributions, it is necessary to assign each event to one final-state mass hypothesis. Some events which have ambiguous assignments can be identified by the ionization density of their tracks while the remaining ambiguous events are assigned to a final state on a probabilistic basis. Unpassed events were assigned in proportion to the passed events. The fraction of events that were probably produced by π mesons was also estimated.

1. Separation of Events by Hypothesis Testing and Ionization Measurement

In order to associate an event with a particular physical process the confidence levels of each fitted hypothesis were compared. After kinematic fitting and an ionization scan, the classification of events by favored (Best) and competing (Next), if any, hypothesis is shown in Table III. As can be seen, a consider-

TABLE III. Ambiguity matrix of two-prong events.

Best / Next	K^-p	$K^-p\pi^0$	K^-pMM	$K^-\pi^+n$	$K^-\pi^+$MM	$p\pi^-\bar{K}^0$	$p\pi^-$MM	$\pi^+\pi^-\Lambda(\Sigma^0)$	$\pi^+\pi^-$MM
K^-p	*4650*	17	0	49	0	0	0	2	0
$K^-p\pi^0$	34	*1039*	11	56	0	266	1	31	0
K^-pMM	1	37	*191*	50	7	93	29	24	6
$K^-\pi^+n$	90	44	2	*894*	4	36	1	512	7
$K^-\pi^+$MM	0	23	462	18	*282*	25	0	82	13
$p\pi^-\bar{K}^0$	0	309	5	48	1	*871*	7	70	0
$p\pi^-$MM	0	18	350	11	97	25	*385*	38	19
$\pi^+\pi^-\Lambda(\Sigma^0)$	3	25	0	832	3	81	0	*1121*	13
$\pi^+\pi^-$MM	1	1	0	92	1221	21	171	62	*1148*
Total	4779	1513	1021	2050	1615	1418	594	1942	1206

able number of events remain ambiguous. This is due largely to the inability to resolve high-momentum (>600 GeV/c) negative tracks. The angular and mass distributions of these ambiguous events were compared with the corresponding distributions of unambiguous events and were found to agree in all essential details. A final state having one or more neutral particles which did not decay or interact in the chamber, may only be inferred from the missing-mass-squared (MM²) distributions, and these events are assigned to the possible final states in proportion to the available phase space.

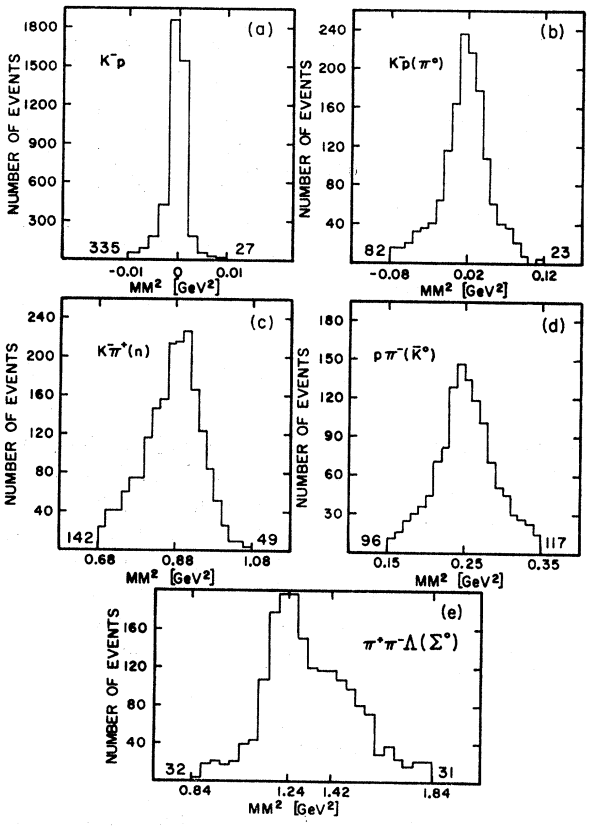

FIG. 2. MM² distributions which had corresponding constrained fits for the final states (a) K^-p, (b) $K^-p\pi^0$, (c) $K^-\pi^+n$, (d) $p\pi^-\bar{K}^0$, and (e) $\pi^+\pi^-\Lambda(\Sigma^0)$. The numbers on the flanks of the histograms represent overflow events not pictured.

For those events that best fit the various two- and three-body hypotheses the MM² distributions are shown in Fig. 2 and are seen to be peaked about the central mass values of the neutral for the respective final states. The width of these distributions is an estimate of the uncertainties associated with the measurements.

2. *Subtraction of Pion-Produced Events*

The total and two-prong cross sections of pion on proton at 2.70 GeV/c are known.[5] To determine the effects of pions in the beam, we measured a sample of two-prong pion induced events at 2.70 GeV/c and fitted the resulting measurements to the kaon hypotheses. It was found that approximately 60% of the measured pion events fitted kaon hypotheses. These pion events which satisfied the elastic-kaon hypothesis exhibited a diffraction peak almost identical to the kaon data obtained after subtraction of the pion effects. The effects of pions on the $\bar{K}\pi N$ inelastic channels generally followed the phase-space distribution and thus were taken into account as part of the background for these three-body final states. Scaling the results of the pion data by the two-prong cross section and the pion contamination in our beam, we were able to determine

TABLE IV. Partial cross sections.

Final state	Raw events	Corrected events	Cross section (mb)
K^-p	4779	5557	6.04±0.30
$K^-p\pi^0$	1513	1368	1.48±0.14
$K^-n\pi^+$	2050	1889	2.05±0.21
$\bar{K}^0p\pi^-$	1418	994	1.07±0.11[a]
$\pi^+\pi^-\Lambda(\Sigma^0)$ for $m\geq 1$	1942	1404	1.52±0.30
$K^-p\pi^0m\pi^0$, $K^-n\pi^+m\pi^0$, $\bar{K}^0p\pi^-m\pi^0$, $\pi^+\pi^-\Lambda(\Sigma^0)$	4436	2000	2.18±0.55
Total	16 138	13 212	14.3 ±0.6

[a] A multiplicative factor of 1.55 will account for the $\bar{K}^0$'s which decay in the chamber and are not analyzed in the two-prong topology. Thus the total $\bar{K}^0p\pi^-$ cross section is 1.66±0.17 mb.

[5] D. H. Miller, L. Gutay, P. B. Johnson, F. J. Loeffler, R. L. McIlwain, R. J. Sprafka, and R. B. Willmann, Phys. Rev. **153**, 1423 (1967).

TABLE V. Measured elastic production angular distribution. One event is 6.9±0.4 μb/sr. Each interval of $\cos\theta_p$ is corrected for biases and pion contamination.

Events	$\cos\theta_p$	$-t$ [(GeV/c)^2]	Events	$\cos\theta_p$	$-t$ [(GeV/c)^2]
2.0± 1.4	−1.000 to −0.975	4.00 to 3.95	6.0± 2.5	0.000 to 0.025	2.00 to 1.95
1.0± 1.0	−0.975 to −0.950	3.95 to 3.90	4.0± 2.0	0.025 to 0.050	1.95 to 1.90
3.0± 1.7	−0.950 to −0.925	3.90 to 3.85	2.0± 1.4	0.050 to 0.075	1.90 to 1.85
0.0± 1.0	−0.925 to −0.900	3.85 to 3.80	6.0± 2.5	0.075 to 0.100	1.85 to 1.80
0.0± 1.0	−0.900 to −0.875	3.80 to 3.75	8.0± 2.8	0.100 to 0.125	1.80 to 1.75
0.0± 1.0	−0.875 to −0.850	3.75 to 3.70	7.0± 2.7	0.125 to 0.150	1.75 to 1.70
0.0± 1.0	−0.850 to −0.825	3.70 to 3.65	5.0± 2.2	0.150 to 0.175	1.70 to 1.65
0.0± 1.0	−0.825 to −0.800	3.65 to 3.60	4.6± 2.8	0.175 to 0.200	1.65 to 1.60
0.0± 1.0	−0.800 to −0.775	3.60 to 3.55	5.0± 2.5	0.200 to 0.225	1.60 to 1.55
1.0± 1.0	−0.775 to −0.750	3.55 to 3.50	9.2± 4.0	0.225 to 0.250	1.55 to 1.50
0.0± 1.0	−0.750 to −0.725	3.50 to 3.45	5.0± 2.5	0.250 to 0.275	1.50 to 1.45
0.0± 1.0	−0.725 to −0.700	3.45 to 3.40	8.6± 3.5	0.275 to 0.300	1.45 to 1.40
1.0± 1.0	−0.700 to −0.675	3.40 to 3.35	10.6± 3.8	0.300 to 0.325	1.40 to 1.35
0.0± 1.0	−0.675 to −0.650	3.35 to 3.30	13.0± 3.8	0.325 to 0.350	1.35 to 1.30
1.0± 1.0	−0.650 to −0.625	3.30 to 3.25	6.0± 2.6	0.350 to 0.375	1.30 to 1.25
2.0± 1.4	−0.625 to −0.600	3.25 to 3.20	3.6± 2.7	0.375 to 0.400	1.25 to 1.20
2.0± 1.4	−0.600 to −0.575	3.20 to 3.15	8.0± 3.0	0.400 to 0.425	1.20 to 1.15
2.0± 1.4	−0.575 to −0.550	3.15 to 3.10	11.6± 3.9	0.425 to 0.450	1.15 to 1.10
3.0± 1.7	−0.550 to −0.525	3.10 to 3.05	7.0± 2.8	0.450 to 0.475	1.10 to 1.05
1.0± 1.0	−0.525 to −0.500	3.05 to 3.00	1.3± 4.0	0.475 to 0.500	1.05 to 1.00
1.0± 1.0	−0.500 to −0.475	3.00 to 2.95	9.6± 3.6	0.500 to 0.525	1.00 to 0.95
0.0± 1.0	−0.475 to −0.450	2.95 to 2.90	13.0± 3.8	0.525 to 0.550	0.95 to 0.90
2.0± 1.4	−0.450 to −0.425	2.90 to 2.85	6.0± 2.6	0.550 to 0.575	0.90 to 0.85
4.0± 2.0	−0.425 to −0.400	2.85 to 2.80	4.6± 2.8	0.575 to 0.600	0.85 to 0.80
5.0± 2.2	−0.400 to −0.375	2.80 to 2.75	9.0± 3.2	0.600 to 0.625	0.80 to 0.75
0.0± 1.0	−0.375 to −0.350	2.75 to 2.70	16.6± 4.5	0.625 to 0.650	0.75 to 0.70
1.0± 1.0	−0.350 to −0.325	2.70 to 2.65	19.0± 4.5	0.650 to 0.675	0.70 to 0.65
5.0± 2.2	−0.325 to −0.300	2.65 to 2.60	8.2± 3.9	0.675 to 0.700	0.65 to 0.60
2.0± 1.4	−0.300 to −0.275	2.60 to 2.55	16.0± 4.1	0.700 to 0.725	0.60 to 0.55
1.0± 1.0	−0.275 to −0.250	2.55 to 2.50	40.6± 6.7	0.725 to 0.750	0.55 to 0.50
4.0± 2.0	−0.250 to −0.225	2.50 to 2.45	55.5± 8.8	0.750 to 0.775	0.50 to 0.45
3.0± 1.7	−0.225 to −0.200	2.45 to 2.40	84.8± 11.1	0.775 to 0.800	0.45 to 0.40
3.0± 1.7	−0.200 to −0.175	2.40 to 2.35	124.5± 12.1	0.800 to 0.825	0.40 to 0.35
6.0± 2.5	−0.175 to −0.150	2.35 to 2.30	168.3± 14.6	0.825 to 0.850	0.35 to 0.30
6.0± 2.5	−0.150 to −0.125	2.30 to 2.25	240.2± 17.8	0.850 to 0.875	0.30 to 0.25
3.0± 1.7	−0.125 to −0.100	2.25 to 2.20	373.0± 23.2	0.875 to 0.900	0.25 to 0.20
6.0± 2.5	−0.100 to −0.075	2.20 to 2.15	541.0± 28.6	0.900 to 0.925	0.20 to 0.15
4.0± 2.0	−0.075 to −0.050	2.15 to 2.10	729.0± 32.4	0.925 to 0.950	0.15 to 0.10
8.0± 2 8	−0 050 to −0 025	2.10 to 2.05	1215.0± 48.0	0.950 to 0.975	0.10 to 0.05
6.0± 2.5	−0.025 to −0.000	2.05 to 2.00	1661.0±173.0	0.975 to 1.000	0.05 to 0.00

their contamination of our data. These contributions were considered when calculating the cross sections and the elastic production angular distribution.

C. Partial Cross Sections

Partial cross sections were calculated after taking into account the detection and measurement biases and the pion contamination. The values used and the results found are displayed in Table IV. In addition to the 14.3±0.6 mb of cross section due to kaon-produced final states whose topologies characteristically appear as two-prong, 2.5 mb of various other kaon-produced topologies appear as two-prong events so that the partial cross section for all final states which appear as two-prong events is 16.8 mb[2].

D. Elastic Production Angular Distribution

The measured elastic production angular distribution in the c.m. system is given in Table V. The preliminary analysis of these data, which did not contain azimuthal corrections, is reported elsewhere.[2] We fitted the production distribution to

$$\frac{d\sigma}{d\omega}=\sum_{n=0}^{N} A_n P_n(\cos\theta_p), \tag{3}$$

where the P_n's are the usual Legendre polynomials. The results after this completed analysis still show no appreciable change in goodness of fit for $N>10$, implying at least $J=\frac{9}{2}$ (i.e., $l=4$) waves must participate.

We also fitted the forward peak to an exponential containing first- and second-order functions of the momentum-transfer squared. The fits of the refined data represent a small change from the originally published data. For

$$\frac{d\sigma}{dt}=\exp\left(\sum_{i=1}^{n} a_i t^i\right), \tag{4}$$

the best fit was obtained for $a_0=3.84\pm0.09$, $a_1=7.52\pm0.25$, and $a_2\cdots a_n=0$.

Viewing the elastic scattering as a diffraction process, we also use the forward portion of our measured elastic

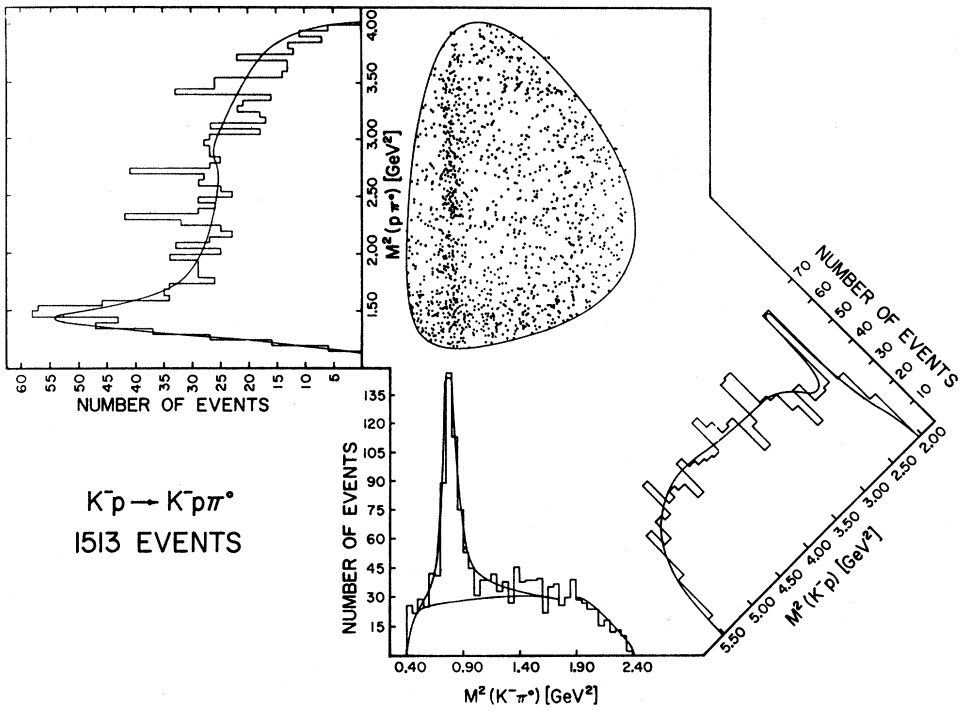

FIG. 3. Dalitz plot and corresponding mass-squared projections for the $K^-p\pi^0$ final state. The upper curve corresponds to the best fit to the data and represents all contributions to the histograms while the lower curve represents the events which were not $\bar{K}^{*-}$.

scattering production angular distribution and the total cross section to obtain the parameters of a specific optical model. For the derivation of this model we refer to the work of Krisch,[6] in which it is assumed that the elastic reaction is dominated by spin-independent absorptive processes. The scatterer is taken to be a grey disk of radius R. A partial-wave analysis is performed in which the phase shift and absorption coefficient for

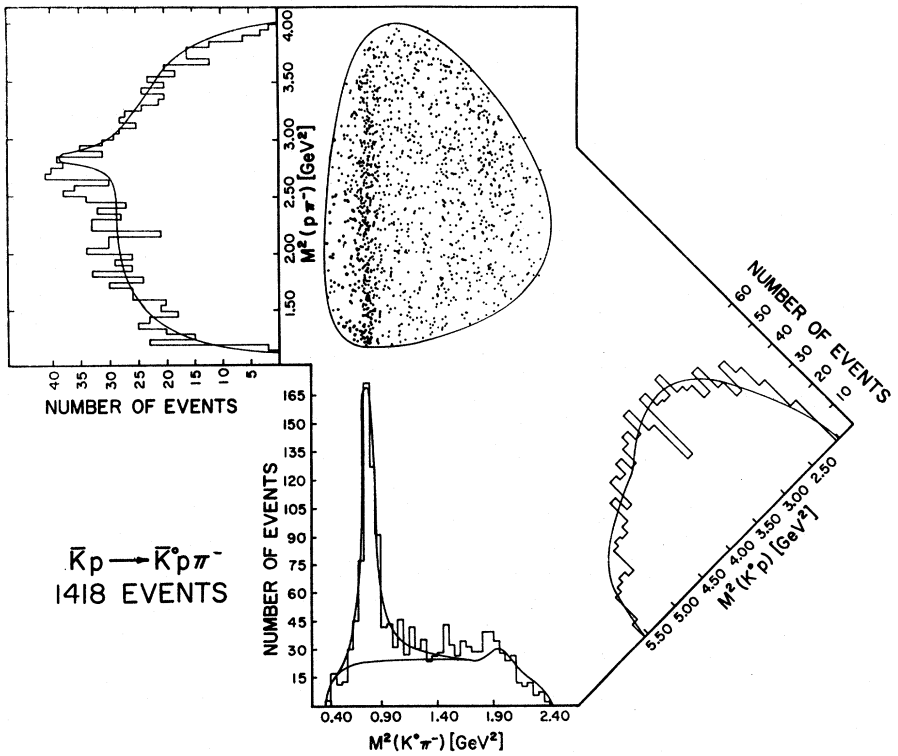

FIG. 4. Dalitz plot and corresponding mass-squared projections for the $\bar{K}^0p\pi^-$ final state. The upper curve corresponds to the best fit to the data and represents all contributions to the histograms while the lower curve represents the events which were not $\bar{K}^{*-}$.

[6] A. D. Krisch, *Lectures in Theoretical Physics* (University of Colorado Press, Boulder, Colo., 1965), Vol. VII-B, p. 249.

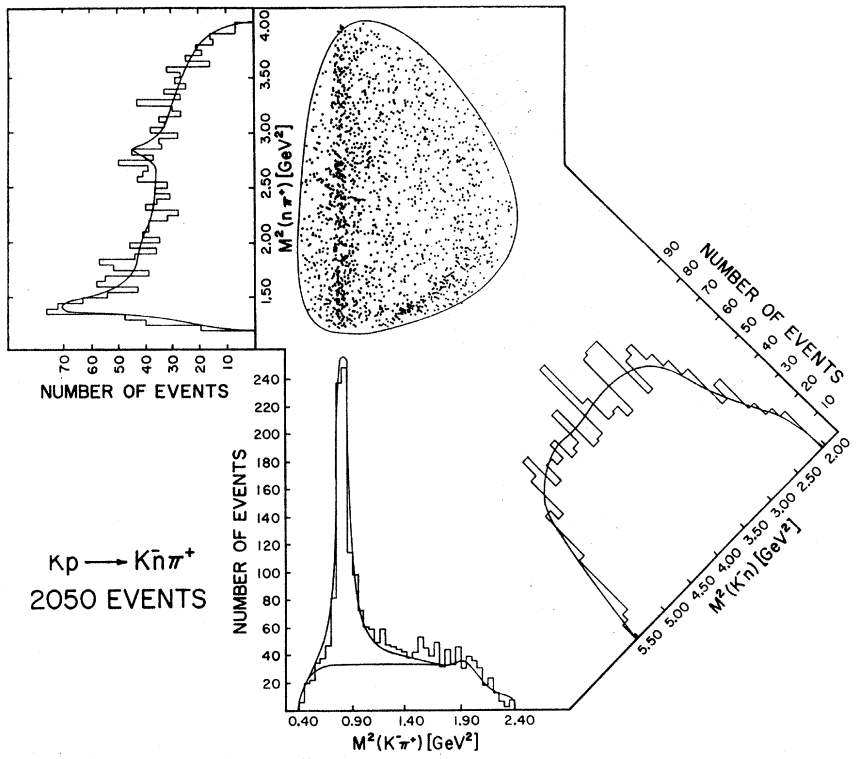

FIG. 5. Dalitz plot and corresponding mass-squared projections for the $K^-n\pi^+$ final state. The upper curve corresponds to the best fit to the data and represents all contributions to the histograms while the lower curve represents the events which were not $\bar{K}^{*0}$.

each partial wave are taken to be independent of l for $0\leq l\leq kR$ and to vanish for $l>kR$. This model then predicts that for c.m. production angles of up to about 70°, the elastic production angular distribution should be

$$\frac{d\sigma}{d\omega}=\alpha(kR^2)^2\left[\frac{J_1(2kR\sin\tfrac{1}{2}\theta_p)}{2kR\sin\tfrac{1}{2}\theta_p}\right]^2. \quad (5)$$

The dashed curve in Fig. 1 is a fit of the differential cross section to that form. The computed elastic cross section for this expression is $\sigma_{el}=\alpha\pi R^2=6.5\pm0.4$ mb, in good agreement with that measured here.

E. $\bar{K}N\pi$ Final States

1. Resonance Production: Masses and Widths

The Dalitz plots and their mass-squared projections for the $K^-p\pi^0$, $\bar{K}^0p\pi^-$, and $K^-n\pi^+$ final states are displayed in Figs. 3–5, respectively. To determine the amount of the contributing resonances, their masses, and their widths, a two-step iterative procedure was used which is described in detail elsewhere.[7] Initially, we considered all the established and suspected resonances which were energetically possible in our data.[8] Table VI summarizes the resulting cross sections. The fitted masses and widths of the $\bar{K}^*$ and $N^*_{3/2}$ are given in Table VII. The experimental resolution, Γ_{rsln}, was obtained from the kinematical analysis program. The approximate relationship

$$\Gamma^2\simeq\Gamma_0^2+\Gamma_{rsln}^2 \quad (6)$$

was used to extract the true width Γ_0. The values found for the mass of both the $\bar{K}^*$ and $N_{3/2}$* are in reasonable agreement with the accepted values.[8] Of interest is the mass difference $\bar{K}^{*0}-\bar{K}^{*-}=10\pm4$ MeV, which is in agreement with results found in a similar analysis at 1.33 GeV/c.[7] However, in both these measurements the experimental resolution is large. These results may be compared with a theoretical prediction for the $\bar{K}^*$ mass difference.[9] The values found for the widths of the resonances are in agreement with the accepted values with the exception of the width of the $N_{3/2}$* in the

TABLE VI. Resonance production cross sections in μb.

	Final state		
	$K^-\pi^0p$	$\bar{K}^0\pi^-p$	$K^-\pi^+n$
$\bar{K}\pi N$ total cross section	1480±140	1660±175	2050±210
$\bar{K}\pi N$ phase space	455±130	507±120	550±193
resonance (M,Γ,M_{ij})			
$\bar{K}_{1/2}$*$(M_{\bar{K}^*},\Gamma_{\bar{K}^*},\bar{K}\pi)$	510±37	934±60	938±45
$N_{3/2}$*$(M_{N^*},\Gamma_{N^*},N\pi)$	352±33	a	355±35
$\bar{K}_{1/2}$*$(1419,89,\bar{K}\pi)$	56±21	122±35	95±25
$N_{1/2}$*$(1470,210,N\pi)$	a	a	51±47
$N_{1/2}$*$(1680,170,N\pi)$	a	97±39	61±24
Y_0*$(1520,16,N\bar{K})$	107±18	a	a

[a] The contribution from this resonance to this final state was less than 1%.

[7] J. R. Ficenec, R. I. Hulsizer, W. P. Swanson, and W. P. Trower, Phys. Rev. **169**, 1034 (1968).

[8] A. H. Rosenfeld, N. Barash-Schmidt, A. Barbaro-Galtieri, L. R. Price, P. Söding, W. S. Willis, and C. G. Wohl, Rev. Mod. Phys. **40**, 1 (1968).

[9] F. Duimio and A. Scotti, Phys. Rev. Letters **14**, 926 (1965).

TABLE VII. Mass and width of the $\bar{K}^*$ and N^*.

Final state	Mass (MeV)	Γ (MeV)	Γ_{rsln} (MeV)	Γ_0 (MeV)
$\bar{K}_{1/2}{}^{*-}$ $(K^-\pi^0)$	890±5	79±13	55	57±13
$\bar{K}_{1/2}{}^{*-}$ $(\bar{K}^0\pi^-)$	892±3	69±9	50	48±9
$\bar{K}_{1/2}{}^{*0}$ $(K^-\pi^+)$	901±1	71±8	50	50±8
$N_{3/2}{}^{*+}$ $(p\pi^0)$	1243±5	370±6	200	310±6
$N_{3/2}{}^{*+}$ $(n\pi^+)$	1209±18	224±13	180	133±13

$K^-p\pi^0$ final state. This may be due to an incorrect estimation of the experimental resolution, but more likely is due to a number of compound resonance and phase-space effects which tend to smear out the $N_{3/2}{}^*$ peak in the $K^-p\pi^0$ final state.

Consideration of the results shown in Table VI and of the data displayed in Figs. 3–5 leads to several observations. First, the only Y^* resonance produced is the $Y_0{}^*(1520)$. Second, although there is a non-negligible contribution of $N_{1/2}{}^*(1470)$ in one final state, the statistical uncertainty is large; therefore, we can not say much for the existence of this resonance in our production reaction. Third, although the $N_{1/2}{}^*(1680)$ appears to be produced somewhat more abundantly than the $N_{1/2}{}^*(1470)$ both contributions are small. Fourth, small amounts of $\bar{K}^*(1419)$ are present in all final states. Fifth, there is a striking absence of $N^*(1238)$ in the $\bar{K}^0p\pi^-$ final state, whereas considerable amounts of $N^*(1238)$ are present in the $K^-p\pi^0$ and $K^-n\pi^+$ final states. Another analysis of the $\bar{K}^0p\pi^-$ final state near our momenta,[10] in which the two-prong-vee topology was studied, found an average cross section of approximately 30–40 μb for the $N^*(1238)$, $N^*(1688)$, $N^*(1512)$, $Y_1{}^*(1660)$, and $Y_1{}^*(1765)$. This is in agreement with the trend seen here. Sixth, the $\bar{K}^*(890)$ dominates all three $\bar{K}\pi N$ final states. It comprises approximately 30, 55, and 47% of the $K^-p\pi^0$, $\bar{K}^0p\pi^-$, and $K^-n\pi^+$ final states, respectively. Comparing the experimental ratio of $\bar{K}^{*-}$ decay in the $\bar{K}^0p\pi^-$ and $K^-p\pi^0$ states with that predicted by isospin conservation of 2, we see that there is excellent agreement:

$$\sigma(\bar{K}^{*-}p\to\bar{K}^0\pi^-p)/\sigma(\bar{K}^{*-}p\to K^-\pi^0p)=1.83\pm0.18.$$

The values we find for the $\bar{K}^0p\pi^-$ and $\bar{K}^{*-}(\bar{K}^0\pi^-)p$ cross sections are in reasonable agreement with those obtained elsewhere.[10]

TABLE VIII. $\bar{K}^*$ production in $\bar{K}N\pi$ final states.

Final state	$\bar{K}^*$ mass interval (GeV)	$\bar{K}^*$ events in mass interval	Background events in mass interval
$\bar{K}^{*0}$ $(K^-\pi^+)n$	0.85–0.95	529	124
$\bar{K}^{*-}$ $(K^-\pi^0)p$	0.84–0.94	290	104
$\bar{K}^{*-}$ $(\bar{K}^0\pi^-)p$	0.84–0.94	347	84

[10] J. H. Friedman and R. R. Ross, Phys. Rev. Letters 16, 485 (1966).

2. *Production and Decay of the $\bar{K}^*(890)$*

The mass interval chosen to represent the $\bar{K}^*$ is given in Table VIII, together with the estimated number of $\bar{K}^*$ and background events it contains. Events in control regions, 50 MeV on either side of the $\bar{K}^*$ mass interval, were subjected to the same analysis as the events within that interval. The background of approximately 20% in the $\bar{K}^*$ region was taken into account in the usual way.[11] The two final states resulting from the decay of the $\bar{K}^{*-}$ were combined for the purposes of the analysis, because their results when taken separately were consistent.

The production angular distributions corrected for background and normalized to include both decay modes of both charge states are shown in Figs. 6(a) and 6(b) for the $\bar{K}^{*0}$ and $\bar{K}^{*-}$, respectively. The distribu-

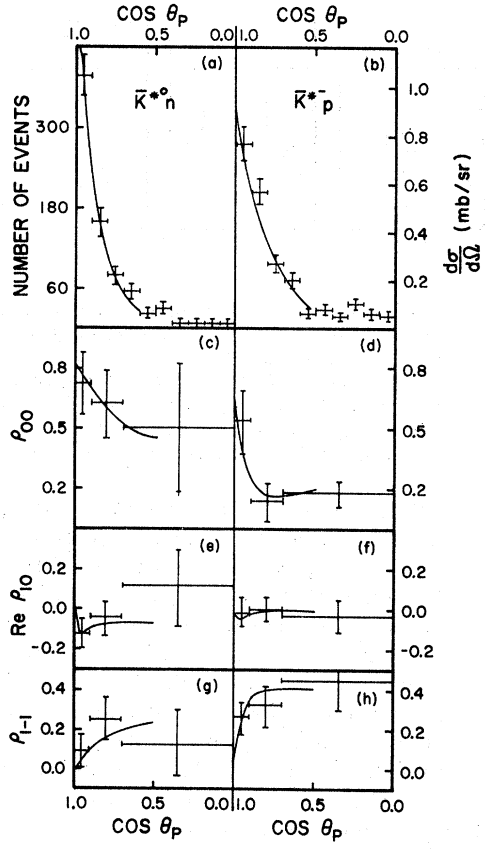

FIG. 6. Center-of-mass production angular distributions for (a) $\bar{K}^{*0}n$ and (b) $\bar{K}^{*-}p$ final states as a function of the $\bar{K}^*$ production cosine ($\cos\theta_p\equiv\hat{P}_{K^-}\cdot\hat{P}_{K^*}$ in the over-all c.m. system) as well as the density matrix element ρ_{00} for (c) $\bar{K}^{*0}$ and (d) $\bar{K}^{*-}$; Reρ_{10} for (e) $\bar{K}^{*0}$ and (f) $\bar{K}^{*-}$; ρ_{1-1} for (g) $\bar{K}^{*0}$ and (h) $\bar{K}^{*-}$. The curve includes contributions from π, ρ, and $\omega(\bar{K}^{*-})$ in the absorption model. All data have been corrected for background.

[11] The expression used for calculating the value of a parameter associated with the $\bar{K}^*$ was $P_{\bar{K}^*}=N_{\text{in}}P_{\text{in}}-N_{\text{out}}P_{\text{out}}/N_{\text{in}}-N_{\text{out}}$, where P_{in} (N_{in}) and P_{out} (N_{out}) are the values of the parameter (number of events) in the $\bar{K}^*$ region and the control region, respectively. The background is relatively flat in both the $\bar{K}^*$ and control regions, so this method should be valid.

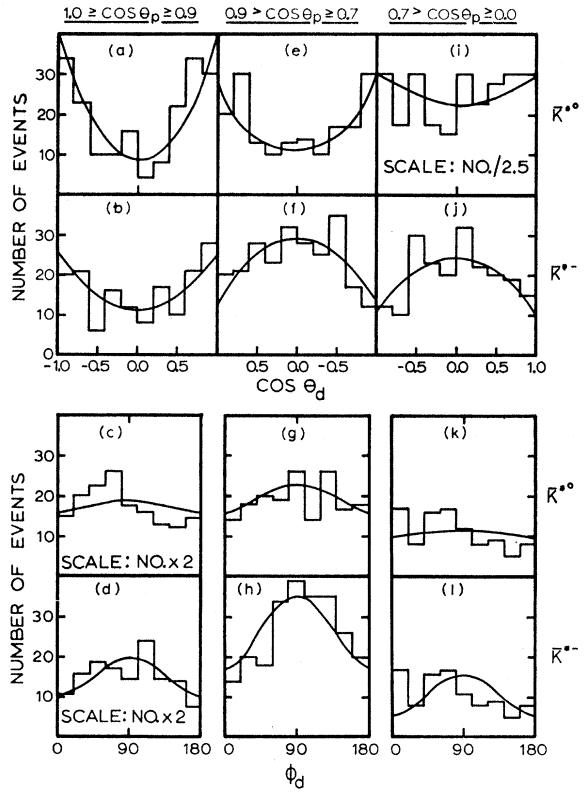

FIG. 7. Fitted decay angular distributions corrected for background in the $\bar{K}^*$ region on the interval $1.0 \geq \cos\theta_p \geq 0.9$ for $\cos\theta_d$ (a) $\bar{K}^{*0}$ and (b) $\bar{K}^{*-}$, for ϕ_d (c) $\bar{K}^{*0}$ and (d) $\bar{K}^{*-}$; on the interval $0.9 \geq \cos\theta_p \geq 0.7$ for $\cos\theta_d$ (e) $\bar{K}^{*0}$ and (f) $\bar{K}^{*-}$, for ϕ_d (g) $\bar{K}^{*0}$ and (h) $\bar{K}^{*-}$; on the interval $0.7 \geq \cos\theta_p \geq 0.0$ for $\cos\theta_d$ (i) $\bar{K}^{*0}$ and (j) $\bar{K}^{*-}$, for ϕ_d (k) $\bar{K}^{*0}$ and (1) $\bar{K}^{*-}$. The angles θ_d and ϕ_d are the usual polar and azimuthal angles associated with the $\bar{K}^*$ decay.

tions are strongly peaked in the forward direction, with the $\bar{K}^{*0}$ distribution falling off more rapidly than the $\bar{K}^{*-}$. These features, which are characteristic of a peripheral-production mechanism, when considered in terms of a meson exchange, suggest that a heavier particle is exchanged more frequently when producing the $\bar{K}^{*-}p$ final state than the $\bar{K}^{*0}n$. The prediction of pion exchange in the peripheral model with absorption was found to be inconsistent with our data ($\chi^2=14.3$ for three data points).[12] For the exchange of an isospin-one particle, the $\bar{K}^{*0}$ and $\bar{K}^{*-}$ production distributions are related by isospin conservation to be

$$\frac{d\sigma}{d\Omega}(\bar{K}^{*-}) = \frac{1}{4}\frac{d\sigma}{d\Omega}(\bar{K}^{*0}). \qquad (7)$$

[12] J. D. Jackson, J. T. Donohue, K. Gottfried, R. Keyser, and B. E. Y. Svensen, Phys. Rev. **139**, B428 (1965); J. T. Donohue, *ibid.* **163**, 1549 (1967); and J. T. Donohue (private communication). This calculation differs from those of the reference in that exact partial-wave sums are used instead of the Bessel-function approximations. The pion coupling constants used were $g_{\bar{K}^{*-}K^-\pi^0}{}^2/4\pi=0.75$ and $G_{pp\pi^0}{}^2/4\pi=14.6$. The solid curves in Fig. 6 for the $\bar{K}^{*0}$ correspond to $X_p=0.16$ and $Y_p=0.6$ and for the $\bar{K}^{*-}$ to $X=2.5$ and $Y=1.1$. In this notation $X=2\xi-\eta$ and $Y=\eta$, where η and ξ are defined in the reference. The values $\gamma_i=0.065$, $\gamma_f=0.049$, $C_i=0.7$, and $C_f=1.0$ were also used in the calculations.

Since both isospin-1 and -0 particles may be exchanged to produce the $\bar{K}^{*-}$, while only isospin-one exchange can be responsible for the $\bar{K}^{*0}$, the measured $\bar{K}^{*-}$ angular distribution when contrasted with the $\bar{K}^{*0}$ distribution is clearly inconsistent with pure isospin-1 exchange, as well as with the pion exchange calculated in the absorption model. The curve in Fig. 6(a) is a prediction of the absorption model, which allows both π and ρ exchange, and agrees much better with the data ($\chi^2=0.7$) than the pure pion fit. The curve in Fig. 6(b) is the prediction of the absorption model based on the data of Friedman and Ross.[10] The agreement is good ($\chi^2=2.3$), and in view of their greater statistics and more constrained topology lends creditability to our efforts.

We have fit the $\bar{K}^*$ angular-decay data by a maximum-likelihood method as a function of production cosine to the general decay angular distribution

$$W(\theta_d,\phi_d) = (3/4\pi)(\rho_{00}\cos^2\theta_d + \rho_{11}\sin^2\theta_d - \sqrt{2}\,\mathrm{Re}\rho_{10}\sin 2\theta_d\cos\phi_d - \rho_{1-1}\sin^2\theta_d\cos 2\phi_d), \qquad (8)$$

where the polar angle θ_d represents the angle between the incoming and outgoing $\bar{K}$ in the c.m. system of the $\bar{K}^*$, while ϕ_d is the Trieman-Yang angle. The resulting density-matrix elements, after correction for background effects, are shown in Figs. 6(c)–6(h). Again for both charge states there is agreement between the data and the absorption-model predictions.

We exhibit the uncorrected data and fits for the decay angular distributions in Fig. 7. Three conclusions can be drawn from these data. First, $\bar{K}^{*0}$ production is dominated by pseudoscalar exchange at all production angles. This is suggested by the symmetric dip in the $\cos\theta_d$ distribution[13] and relatively flat ϕ_d distribution. Second, $\bar{K}^{*-}$ production is dominated by pseudoscalar exchange in the forward direction, while vector exchange dominates at larger production angles. This is suggested by the $\cos^2\theta_d$ character of the $\cos\theta_d$ distribution for $1.0 \geq \cos\theta_p \geq 0.9$ and the $\sin^2\theta_d$ character for $\cos\theta_p < 0.9$. In addition the ϕ_d distribution is nonisotropic and strongly resembles $1-\cos 2\phi_d$. Finally, no strong asymmetries are noted in the data, suggesting little interference between $\bar{K}^*$ and background amplitudes.

Thus we conclude from the $\bar{K}^{*0}$ and $\bar{K}^{*-}$ production and decay distributions that pseudoscalar exchange with possibly a slight amount of vector exchange is responsible for the $\bar{K}^{*0}$ production, while both pseudoscalar and vector exchange contribute significantly to the $\bar{K}^{*-}$ production. Therefore, the vector exchange must be dominantly isoscalar in the $\bar{K}^{*-}p$ final state. We now use the data from the $\bar{K}^{*0}n$ state to determine the isovector and isoscalar contributions to this vector exchange for the $\bar{K}^{*-}p$ state. If only pseudoscalar

[13] For the $\cos\theta_d$ distributions the forwardmost bin in production cosine has been corrected.

exchange were responsible for $\bar{K}^{*0}$ production, then only an isoscalar contributes to the vector exchange in the $\bar{K}^{*-}p$ state. However, the absorption-model fit which includes ρ exchange is more representative of our $\bar{K}^{*0}n$ data. The results of these fits indicate that the contribution to the cross section from ω exchange is more than ten times that of ρ.

The general features of our data have also been noted in another K^-p experiment and in a K^+d experiment,[14] both at lower energies. To refine the results reported here, increased statistics are needed, as even relatively small errors allow a large range of parameters in any model.

[14] S. Goldhaber, J. L. Brown, I. Butterworth, G. Goldhaber, A. A. Hirata, J. A. Kadyk, and G. H. Trilling, Phys. Rev. Letters **15**, 737 (1965).

F. $\pi^+\pi^-\Lambda(\Sigma^0)$ Final States

No detailed analysis of the $\Lambda\pi^+\pi^-$ or the $\Sigma^0\pi^+\pi^-$ final states was attempted, since over 40% of the data represents contamination.

ACKNOWLEDGMENTS

We wish to acknowledge the useful discussions and the calculations of the absorption curves by Dr. J. T. Donohue. We thank Professor E. L. Goldwasser and Professor R. I. Hulsizer for their continued support and encouragement throughout this experiment, and Purdue University for the use of their π^- film. The privilege of participating in this collaboration with the Alvarez group at the Lawrence Radiation Laboratory is gratefully acknowledged.

PHYSICAL REVIEW VOLUME 175, NUMBER 5 25 NOVEMBER 1968

Search for a Strange Boson of Mass Less than 670 MeV

LAWRENCE KIRSCH*
Brandeis University, Waltham, Massachusetts
(Received 22 July 1968)

The cross section for the production of a strange boson in the mass region 565 to 670 MeV in the reaction $K^-p \to p\kappa^-$ is found to be less than 11 μb with 95% confidence. A crude theoretical estimate of the cross section based upon a simple pole model yields 11 μb.

IT has been proposed[1] that there may exist a scalar kaon (κ) which has a mass less than 670 MeV and may in fact lie below the $K\pi$ threshold. The principal decay mode of such a particle would be $\kappa \to K\gamma\gamma$. We have searched for such a particle in the reaction $K^-p \to \kappa^-p$ and find that the cross section for this process is less than 11 μb in the mass region 535 to 670 MeV.

The experiment is based on the analysis of 3×10^4 pictures of the Brookhaven National Laboratory 31-in. hydrogen bubble chamber exposed to a 2.88-GeV/c K^- beam at the AGS. The film was scanned for all K^- interactions producing two prongs where the positive track was identified as a proton by ionization. Two-prong events with a "V" resulting from a K^0 decay were also accepted. After various fiducial-volume requirements were applied to the data, there remained 4880 events.

These events are primarily from the reactions

$$\begin{aligned} K^-p &\to pK^- \\ &\to pK^{*-} \to p\bar{K}^0\pi^- \\ &\qquad\quad \searrow pK^-\pi^0 \\ &\to p\pi^-K^0 \end{aligned}$$

or reactions where additional neutral particles are produced. In order to reduce the background in the κ-mass region, we have selected a sample of events for which the protons have a center-of-mass scattering angle in the range $0.9<\cos\theta^*<1.0$. This limits the laboratory momentum of the proton to 540 MeV/c for the elastic events, and to 495 MeV/c for events in the K^* mass region, ensuring positive identification of the proton track. There are 3036 events which satisfy this criterion. The mass recoiling against the proton for those events in the region below 1 GeV is shown in Fig. 1. All further discussion will be restricted to this sample of events.

The sensitivity of this experiment has been determined by comparing the observed number of events in the elastic peak with the measured cross section for this process.[2] This yields a sensitivity of 1.6 μb/event. As a check of this conversion factor, we note that the measured value of the K^{*-} cross section[3] predicts that 255 ± 52 events are expected in this data. This is consistent with the 220 ± 40 K^* events observed.

The 245 events in the mass interval 520–670 MeV were carefully remeasured, and the missing mass for the events remaining in this region after remeasurement is shown in Fig. 2.

Since there is no reliable estimate of the background from elastic events, we assume no background, and use

* Work supported by the U. S. Atomic Energy Commission under Contract No. AT(30-1)3178.
[1] S. L. Glashow and Steven Weinberg, Phys. Rev. Letters **20**, 224 (1968).
[2] M. N. Focacci *et al.*, Phys. Letters **19**, 441 (1965).
[3] R. Barloutaud *et al.*, Phys. Letters **12**, 352 (1964).